Journal of Micromechanics and Microengineering

On-chip enucleation of an oocyte by untethered microrobots

OPEN ACCESS
IOP Publishing
Journal of Micromechanics and Microengineering
J. Micromech. Microeng. **24** (2014) 095004 (8pp)
doi:10.1088/0960-1317/24/9/095004

On-chip enucleation of an oocyte by untethered microrobots

Akihiko Ichikawa[1], Shinya Sakuma[2], Masakuni Sugita[3], Tatsuro Shoda[3], Takahiro Tamakoshi[3], Satoshi Akagi[4] and Fumihito Arai[3]

[1] Department of Mechatronics Engineering, Graduate School of Engineering, Meijo University, 1–501 Siogamaguchi, Tenpaku, Nagoya, Aichi, 468–8502, Japan
[2] Department of Mechanical Engineering, Graduate School of Engineering, Osaka University, 2-1 Yamadaoka, Suita, 565–0871, Japan
[3] Department of Micro-Nano Systems Engineering, Nagoya University, Furo-cho, Chikusa-ku, Nagoya, Aichi, 464–8603, Japan
[4] Animal Breeding and Reproduction Research Division, NARO Institute of Livestock and Grassland Science, 2 Ikenodai, Tsukuba, Ibaraki 305–0901, Japan

E-mail: ichikawa@meijo-u.ac.jp

Received 30 January 2014, revised 22 April 2014
Accepted for publication 14 May 2014
Published 31 July 2014

Abstract
We propose a novel on-chip enucleation of an oocyte with zona pellucida by using a combination of untethered microrobots. To achieve enucleation within the closed space of a microfluidic chip, two microrobots, a microknife and a microgripper were integrated into the microfluidic chip. These microrobots were actuated by an external magnetic force produced by permanent magnets placed on the robotic stage. The tip of the microknife was designed by considering the biological geometric feature of an oocyte, i.e. the oocyte has a polar body in maturation stage II. Moreover, the microknife was fabricated by using grayscale lithography, which allows fabrication of three-dimensional microstructures. The microgripper has a gripping function that is independent of the driving mechanism. On-chip enucleation was demonstrated, and the enucleated oocytes are spherical, indicating that the cell membrane of the oocytes remained intact. To confirm successful enucleation using this method, we investigated the viability of oocytes after enucleation. The results show that the production rate, i.e. the ratio between the number of oocytes that reach the blastocyst stage and the number of bovine oocytes after nucleus transfer, is 100%. The technique will contribute to complex cell manipulation such as cell surgery in lab-on-a-chip devices.

Keywords: microrobot, mems, biomiro, micro-fluidic chip

(Some figures may appear in colour only in the online journal)

1. Introduction

In the biomedical engineering field, complex cell manipulation, such as cell surgery, is in high demand for analyzing cell properties and evaluating drug efficacies [1]. Some of the most complicated cell surgeries are cloning techniques [2]. There is increasing demand for cloning techniques for maintaining sufficient food supply, developing medical treatment applications such as organ transplantation, and developing genetically similar laboratory animals. Generally, two types of cloning technique are widely used, the Roslin technique or Honolulu technique [3]. The Roslin technique was used for cloning 'Dolly' the sheep. This technique utilizes the nucleus of a somatic cell as a donor cell. On the other hand, the Honolulu technique utilizes embryo nuclei as donors [4]. These techniques are based on the same three-step procedure: (I) enucleation, (II) donor cell injection, and (III) fusion of the original oocyte and the injected

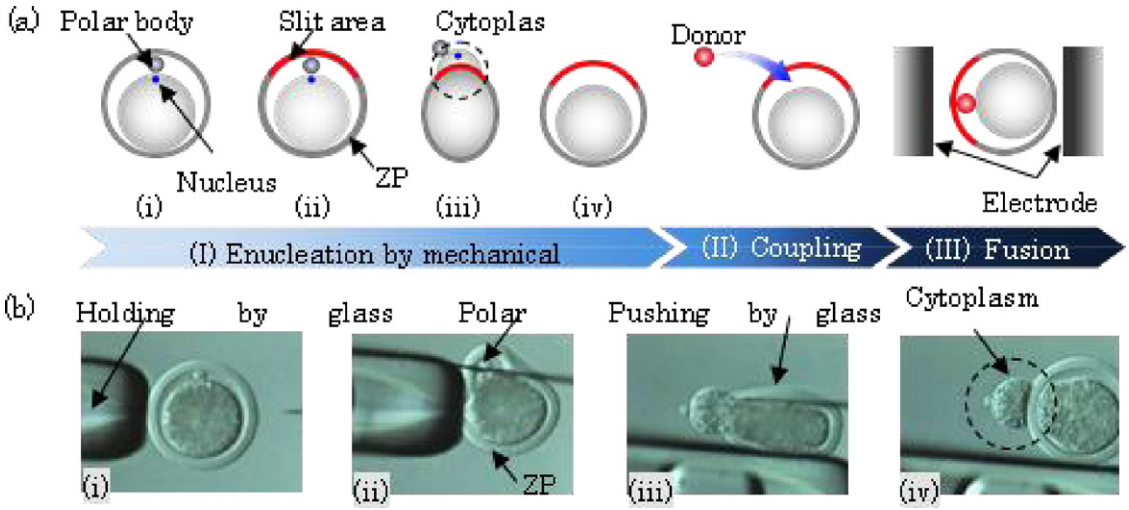

Figure 1. Process of cloning. (*a*) General protocol for cloning; (*b*) enucleation of oocyte manually. (*i*) Holding of oocyte; (*ii*) penetration of zona pellucida (ZP); (*iii*) enucleation by pushing cellular cytoplasm out of ZP; and (*iv*) enucleated oocyte (Takahashi *et al*, NAFR, Japan).

donor cell. Details of the cloning process are summarized as follows. Firstly, an oocyte is aspirated and held by a glass capillary (figure 1(*i*)). Secondly, the oocyte is penetrated and cut by a glass needle (figure 1(*ii*)). Thirdly, the nucleus included in the cytoplasm is pushed out of the zona pellucida (ZP) (figure 1(*iii*)). A donor cell is then injected into the oocyte (figure 1(*iv*)). Finally, the oocyte and donor cell are fused by applying voltage. Enucleation without the use of toxic fluorescent dye increases the production rate and is a minimally invasive operation. A polar body is used as an enucleation target without using any fluorescent dye, because the polar body is most likely next to the nucleus of the oocyte, which is in maturation stage II [5]. Therefore, removal of the polar body and a small ambient area are sufficient to complete the enucleation.

The conventional cloning process is carried out using glass capillaries attached to mechanical micromanipulators as end effectors that have various functions, such as holding and cutting. In addition, a mechanical micromanipulator with robot technology is capable of precise operation, high output force and multiple degrees of freedom (multi-DOF). Consequently, the complicated cloning process is mainly conducted manually by operators. Although mechanical micromanipulators with multi-DOF can manipulate a cell by using complex procedures, the manipulation requires highly skilled operators because the manipulators must be controlled in multi-DOF. Therefore, the success rate, repeatability and productivity of manipulations tend to depend on the operator's skill, especially for complex procedures like cloning. Moreover, the manipulators are placed outside the cell culture environment, where they are exposed to air. This can lead to several problems, including contamination.

On the other hand, lab-on-a-chip devices employ a closed environment, such as microchannels and microchambers. This type of configuration prevents cell contamination and restricts the position of cells in a two-dimensional plane. Moreover, the mass production of disposable microfluidic chips lowers their cost. Therefore, we proposed on-chip cloning and reported the effectiveness of on-chip enucleation using fluid force in a previous study [6]. The enucleation was automated by utilizing real-time feedback control of the robotic pump based on image analysis [7]. This automation system achieved high throughput with high repeatability. However, the method required removal of the ZP from the oocyte [7, 8]. High speed-enucleation using a microrobot was also performed with a non-ZP oocyte [9]. The ZP plays vital roles during oogenesis, fertilization and preimplantation development [10]. Therefore, an enucleation method that includes the ZP is highly required for biomedical applications.

In this paper, we propose a novel on-chip enucleation of an oocyte with ZP by untethered microrobots. To achieve on-chip enucleation, we integrate the advantages of a mechanical manipulator and lab-on-a-chip devices. The untethered microrobots, which have a gripping or knife function, are packaged in a microfluidic chip and actuated by the external magnetic force generated by permanent magnets placed on the robotic stage. In section 2, the details of each untethered microrobot are described by considering the requirements for on-chip enucleation. Section 3 outlines the evaluation results of the microrobots. Moreover, on-chip enucleation of a bovine oocyte with ZP is demonstrated by the combination of the untethered microrobots in a microfluidic chip. Finally, the conclusions and our future plans are presented in section 4.

2. Materials and methods

2.1. Untethered microrobots for on-chip enucleation

Enucleation, as described in section 1, is mainly divided into three processes, (a) holding, (b) penetrating and cutting an oocyte, and (c) removing the nucleus and some cellular cytoplasm. The most important requirement is the output force, because an output force on the order of several hundred micronewtons is required to deform an oocyte. There are several different types of microactuator that can be applied in the confined space of microchannels, including bubble

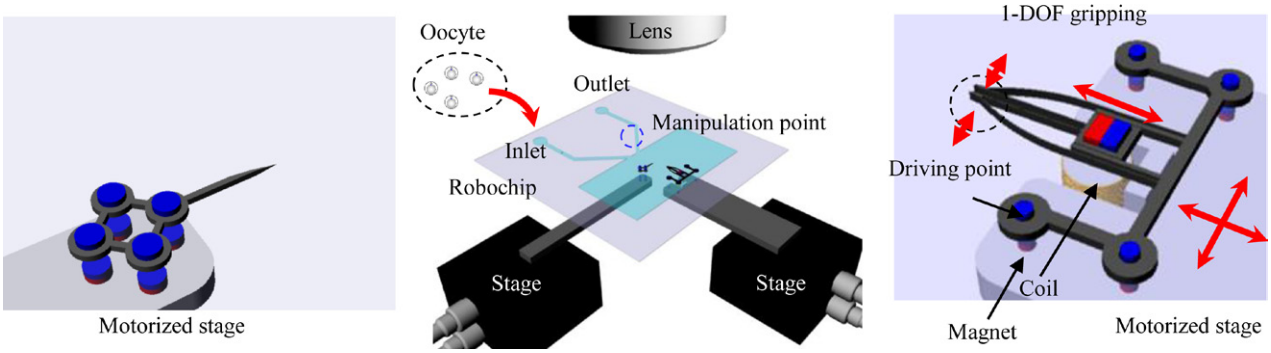

Figure 2. Conceptual view of the robochip and the on-chip enucleation system.

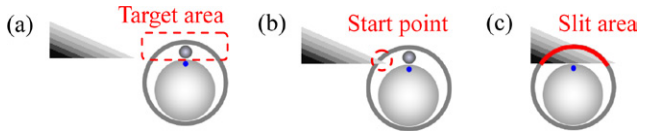

Figure 3. Cutting sequence. (*a*) Approaching target oocyte; (*b*) penetrating oocyte; and (*c*) slitting the ZP.

actuators driven by thermocapillary flow [11], optical tweezers [12] and magnetic microactuators [13]. Among the many different microactuation mechanisms, magnetic actuation has certain advantages over other methods for an on-chip microactuator due to the suitable source of the force [14, 15]. Thus, considerable research has been carried out on magnetic actuators for cell manipulators. Previously [8, 9, 13, 16–18], we proposed a magnetically driven microtool (MMT) for on-chip cell manipulation. Magnetic actuation enables manipulation of cells in a closed microfluidic chip by forces on the order of millinewtons. Therefore, we applied a magnetically driven method to actuate the untethered microrobots because of its noncontact actuation capability and high output force for on-chip enucleation.

A conceptual view of the on-chip enucleation system is shown in figure 2. The system contains two motorized stages, a microfluidic chip and a sensing part that is based on a CCD camera attached to the optical microscope. The microfluidic chip has two untethered microrobots, a microgripper and a microknife, which are driven by the magnetic force produced by the permanent magnets placed on the motorized stages. Oocytes are transported to the manipulation point in a microfluidic chip by the flow. The oocytes are then enucleated by the two microrobots. The enucleation process is subdivided into three steps: (a) holding, (b) slitting, and (c) removing the nucleus. The required DOF of the microrobot in each step is summarized as follows.

(a) *Holding*: the microgripper requires at least 2-DOF motion in a plane to approach the oocyte. An additional 1-DOF actuation is required to accomplish the gripping function.
(b) *Slitting*: the microknife requires at least 2-DOF motion to approach the nucleus of the oocyte. The slitting function is achieved with relative 1-DOF motion between the microknife and microgripper, as shown in figure 3; although the slitting function is based on the penetration and cutting motion.
(c) *Removing the nucleus*: the microrobot should be actuated with at least 1-DOF motion to push the nucleus with cytoplasm out of the ZP. This 1-DOF motion can be achieved using the griping motion of the microgripper.

The concept and design of each microrobot is described in the following sections.

2.2. Microknife

As mentioned in section 2.1, the microknife requires 2-DOF motion to approach the nucleus of the oocyte. Furthermore, in the case of a microrobot having a knife probe, a slitting function is possible with relative 1-DOF motion. Concept images of the cutting sequence are shown in figures 3(*a*)–(*c*). Firstly, a microrobot approaches the nucleus of the oocyte (figure 3(*a*)). The microrobot subsequently penetrates the ZP by using the sharp tip (figure 3(*b*)). While the microrobot is penetrating the ZP, the knife-like structure slits open the ZP (figure 3(*c*)). To design the microknife, a model of slitting is considered, as shown in figure 4. The most important parameter of the knife is the relationship between the angle of the knife tip ϕ and the required manipulation stroke L. Here, we considered the case that L is maximized when the cytoplasm of the oocyte is located at the edge of the ZP. Moreover, we assumed that the deformation of the oocyte can be ignored to consider the case of maximized L. When ϕ' is small $\left(L < \sqrt{D^2 - l^2}\right)$, the end point of the slitting is on the cutting edge of the microknife. On the other hand, when ϕ' is large $\left(L \geq \sqrt{D^2 - l^2}\right)$, the end point is on the tip of the microknife. Therefore, the following relationship is satisfied between ϕ and L.

$$L = \begin{cases} \dfrac{D/2}{\sin\varnothing} + \dfrac{\delta}{\cos\varnothing} - \dfrac{\delta}{\sin\varnothing\cos\varnothing} + \sqrt{D^2-\delta^2} & , L < \sqrt{D^2-\delta^2} \\ \sqrt{D^2-\delta^2} & , L \geq \sqrt{D^2-\delta^2} \end{cases} \quad (1)$$

where, D is the diameter of the oocyte, d is the diameter of the cytoplasm, t is the thickness of the ZP and δ is a parameter determined by equation (2).

$$\delta = d + t - D/2 \quad (2)$$

The relationship is calculated as shown in figure 5. The vertical axis shows the required stroke and the horizontal axis shows the tip angle of the microknife. In this calculation, D, d and t for the enucleation of a bovine oocyte are: $D = 150\,\mu$m, $d = 80$, $110\,\mu$m, $t = 15\,\mu$m. These values are obtained from observation

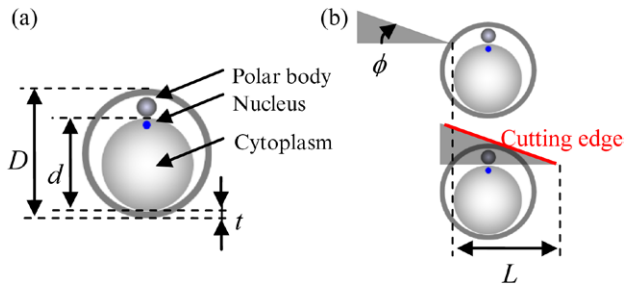

Figure 4. Analytical model of slitting oocyte. (*a*) Parameters of the oocyte and (*b*) analytical model of required stroke L as a function of tip angle ϕ.

of the oocyte. To adapt the microknife to enucleation of various d, ϕ and L are designed as 10° and 550 μm, respectively.

2.3. Microgripper

The microgripper is actuated by external magnetic force to achieve noncontact actuation with high output force, as shown in figure 2. Specifically, four driving points of permanent magnets are vertically arranged in the microgripper for 2-DOF actuation. These magnets are driven by the external magnetic force of magnets on the motorized stage. To achieve the additional 1-DOF gripping motion, a horizontally arranged permanent magnet is placed at the center of the microgripper. This magnet is driven by the magnet field of the electromagnetic coil, which is placed on the motorized stage. Thus, the microgripper picks up target cells one by one and pushes the cells using a gripping motion.

2.3.1. Design of the gripping mechanism. The gripping mechanism is performed by the deformation of beams because it is difficult to achieve an ideal microscale hinge-and-link structure. Figure 6(*a*) shows the deformation model of the gripping mechanism when the driving force F is applied to the horizontally arranged permanent magnet.

First, to obtain the gripper's tip deformation δ_X and δ_Y caused by applied force F, the gripping mechanism is considered as half of the frame structure. Point A is the base of the frame connected the gripper's body, point B is the tip of the gripper and point C is driven by the magnetic force, as shown in figure 6(*b*). F_x, and M are the virtual load along the x axis for point A, and the moment around point A, respectively.

Here, the structure of the microgripper is considered an elastic material. The elastic strain energy U is expressed by equation (1) under the assumption that the deformation due to compression and the torsion of each beam is ignored.

$$U = U_{AB} + U_{BC} \tag{3}$$

Where U_{AB} and U_{BC} are the elastic strain energy of the beams, and expressed as follows:

$$U_{AB} = \int_0^{l_1} (M_{AB})^2 dr_1,\ U_{BC} = \int_0^{l_2} (M_{BC})^2 dr_2, \tag{4}$$

Where r_1, r_2 l_1 and l_2 are divided segments along the beams, and the total length of the beams, respectively. M_{AB} and M_{BC} are the moments around point A and C, respectively. M_{AB} and M_{BC} are described as follows:

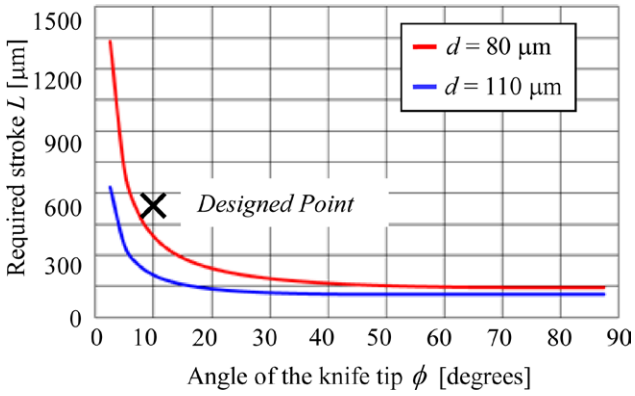

Figure 5. Required stroke L as a function of tip angle ϕ.

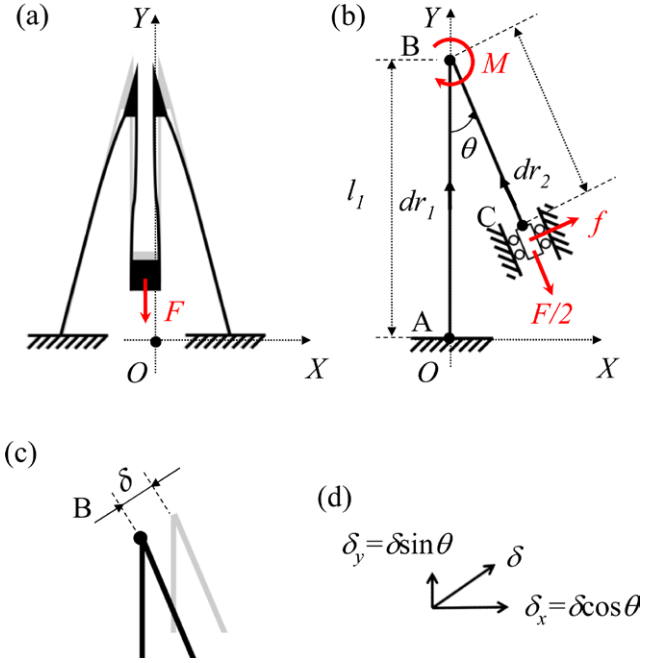

Figure 6. Analytical model of gripping mechanism. (*a*) Deformation model; (*b*) half of frame model; (*c*) enlarged view around point B; and (*d*) definition of δ_x and δ_y.

$$M_{AB} = (F_x + F/2 \sin\theta - f\cos\theta)\, r_1 + fl_2 - M \tag{5}$$

$$M_{BC} = -M + fr_2 \tag{6}$$

Here the f is the vertical component of force $F/2$ as shown in figure 6(*b*).The displacement of the gripper tip is given as equation (7) under the boundary condition expressed by equation (8). Where, θ, E and I are the angle between the beams of the tip, Young's module of the frame and the second moment of the beam, respectively.

$$\delta = \frac{l_1^3 l_2^3 (l_1 + l_2) \sin\theta F}{3EI\left(l_1^4\cos^2\theta + 4l_1^3 l_2 \cos^2\theta - 6l_1^2 l_2^2 \cos\theta + 4l_1 l_2^3 + 4l_2^4\right)} \tag{7}$$

$$\left(\frac{\partial U}{\partial M}\right)_{F_x=0} = 0,\ \left(\frac{\partial U}{\partial f}\right)_{F_x=0} = 0,\ \delta = \frac{\partial U}{\partial F_x}, \tag{8}$$

Therefore, δ_X and δ_Y are obtained by equation (9).

$$\delta_X = \delta\cos\theta,\ \delta_Y = \sin\theta \tag{9}$$

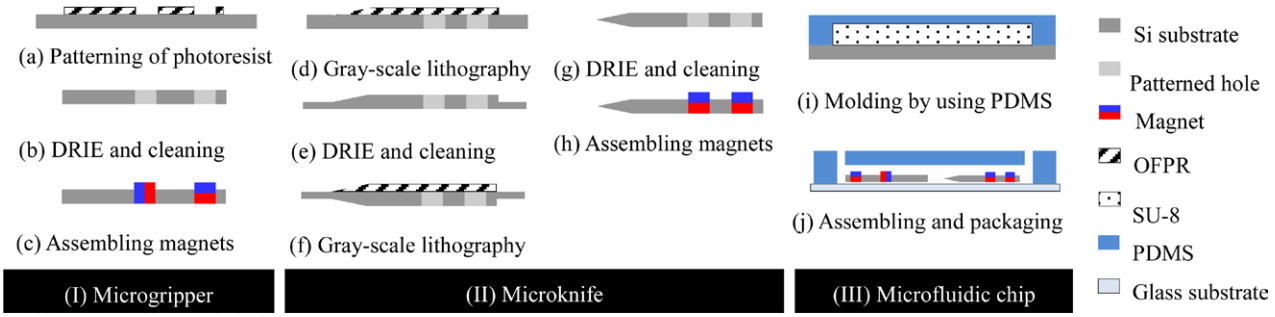

Figure 7. Analysis of gripping mechanism. (*a*) Gripping displacement as a function of tip angle, and (*b*) partial enlargement of vertical axis of graph (*a*) in the region of 0–160 μm.

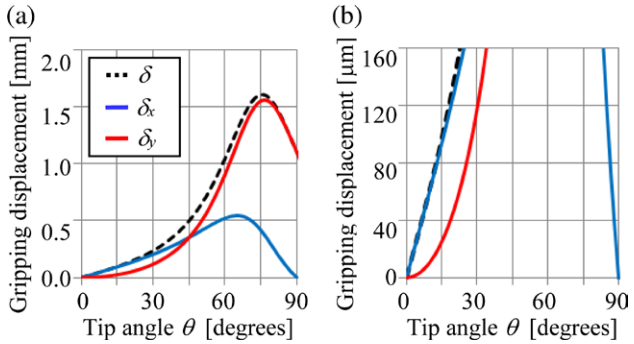

Figure 8. Fabrication process of microrobots and microfluidic chip.

The analytical results are shown in figure 7. In this calculation, the value of l_1 and l_2 are designed as 6.5 mm and 3.3 mm, respectively, because the light of the microscope through from the bottom of the microrobot and the electrical magnet interrupts the light. Considering that the bovine oocyte is approximately 150 μm in diameter, we designed the distance between the tip of the gripping mechanism to be 160 μm. To close the tip of the gripper perfectly, δ_X must be over 80 μm. Therefore, we designed the angle to be 13 °.

2.4. Fabrication of the microrobots and the microfluidic chip

To create the microfluidic chip containing the microrobots, the fabrication process is based on a simple two-step procedure. First, the microgripper, microknife and microchannel were fabricated identically. The components of the microfluidic chip were then assembled and packaged. Figure 8 shows the fabrication processes of the microgripper, microknife and microfluidic chip.

2.4.1. Fabrication of the microgripper. (a) A photoresist (OFPR, Tokyo Ohka Co Ltd) layer was patterned on the Si substrate for the deep reactive ion etching (DRIE) mask. The Si substrate was utilized as the material for the microgripper. (b) Hole patterns were fabricated using DRIE. The photoresist pattern was then removed by O_2 plasma ashing.

(c) Permanent magnets were assembled on the hole patterns. Vertically arranged magnets were adopted as the driving part for 2-DOF lateral motion and a horizontally arranged magnet was adopted for the gripping motion.

2.4.2. Fabrication of the microknife. (d) OFPR was patterned using grayscale lithography after making the hole pattern in the same manner as the microgripper. Grayscale lithography is a photolithography technique for fabricating three-dimensional (3D) microstructures [19].

(e) The 3D shape of the microknife was transcribed by DRIE because of the difference in the etching rate between the Si substrate and the photoresist.

(f), (g) The opposite side of the microknife was fabricated by grayscale lithography and DRIE.

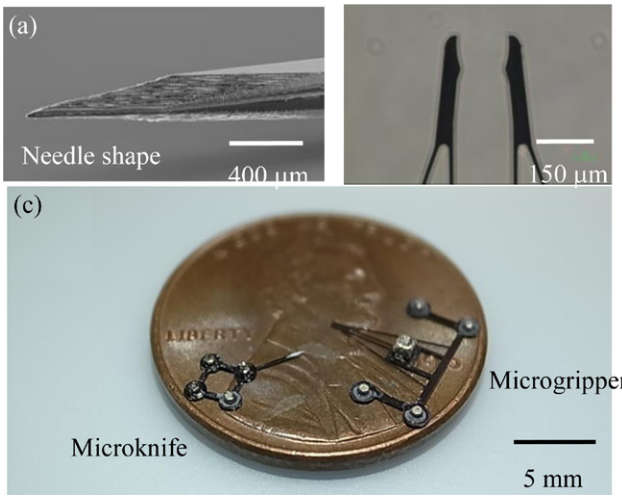

Figure 9. Images of fabricated microrobots. (*a*) SEM image of tip of microknife; (*b*) photograph of the microgripper tip; (*c*) photograph of the fabricated microrobots.

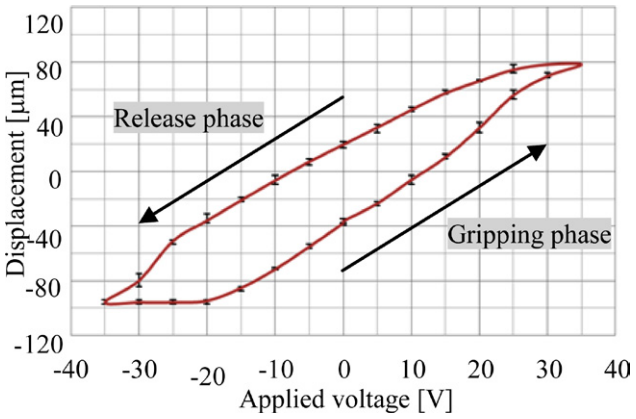

Figure 10. Measured manipulation band as a function of the voltage applied to the electromagnetic coil.

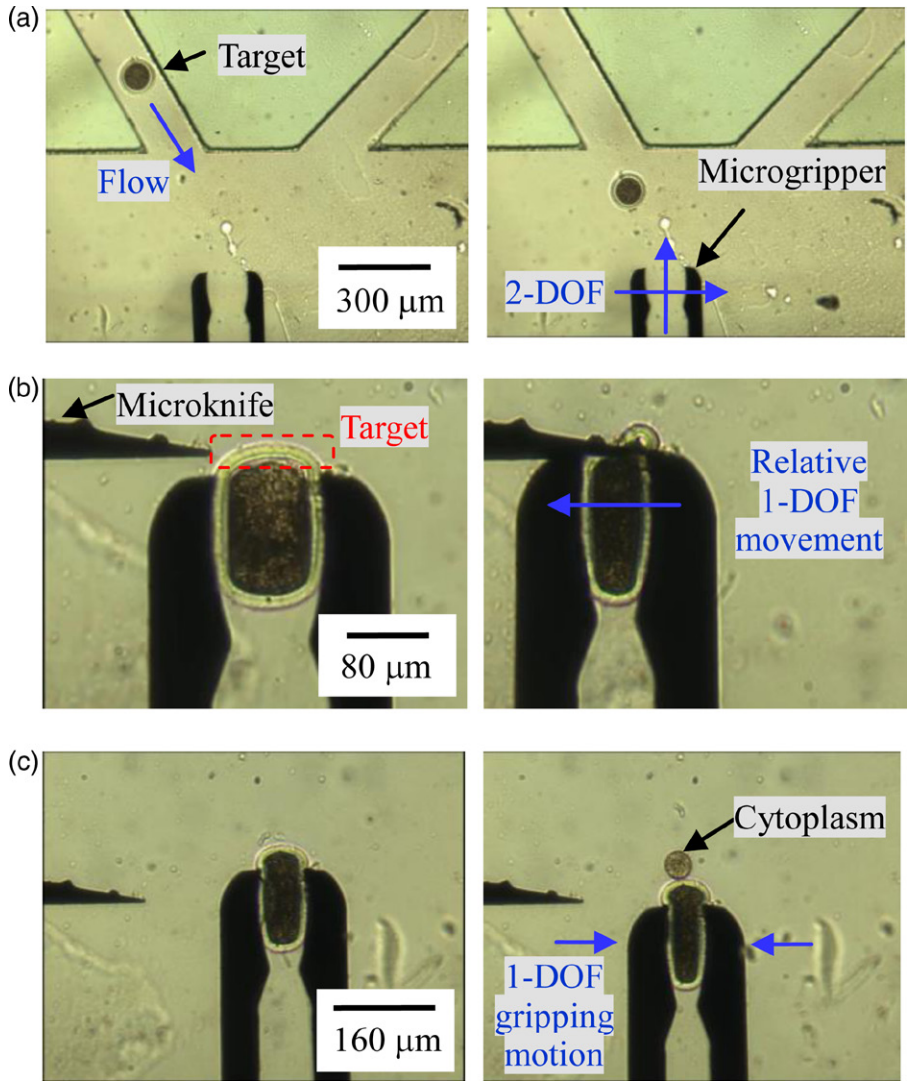

Figure 11. Demonstration of on-chip enucleation using the microknife and the microgripper.

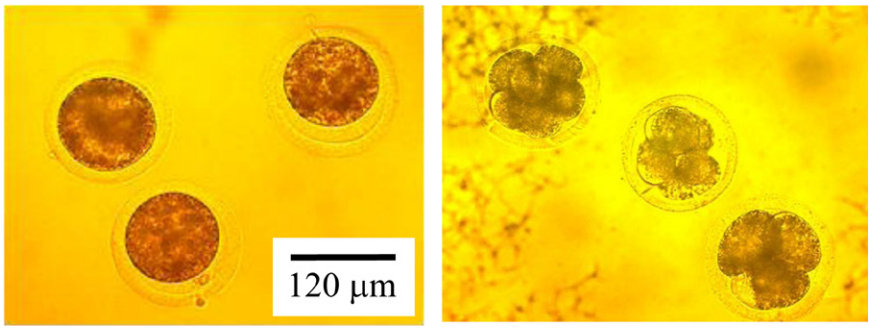

Figure 12. Experimental results of enucleation process. (*a*) Enucleated oocytes and (*b*) 5-day-cultured oocytes after cloned donor cell.

(h) Permanent magnets were assembled on the hole patterns for 2-DOF lateral motion.

2.4.3. Fabrication of the microfluidic chip. (i), (j) The cover of the microfluidic chip was fabricated by moulding poly(dimethylsiloxane) (PDMS). The microchannel mould was patterned using SU-8 (Nippon Kayaku Co Ltd). The fabricated microrobots were then assembled on the microfluidic chip and packaged.

Images of the fabricated microknife and microgripper are shown in figure 9.

3. Experiment

3.1. Evaluation of the microgripper

The fabricated microgripper was evaluated in terms of the manipulation stroke, which is the tip displacement of the microgripper. The manipulation stroke was measured as a function of the applied voltage of the electromagnet coil (RZ-48 W, B5, Fujitsu Ltd), as shown in figure 10. The vertical axis shows the tip displacement on one side. The line shows the average value of four measurements, and the upper

and lower error bar shows the maximum and minimum values, respectively. The displacement was measured by the image taken from the CCD camera attached to the microscope. The results indicate that the gripper has a hysteresis between the gripping phase and release phase and that there is a relatively linear relationship between the tip displacement and applied voltage when the applied voltage is between –20 V and 20 V. The causes of the hysteresis are the friction between the bottom of the microgripper and the surface of the glass plate of the microfluidic chip. In addition, the maximum and minimum errors are –3.5 μm and 4.3 μm, respectively. From these results, we concluded that the manipulation stroke is 160 μm during the gripping phase, which was sufficient for on-chip enucleation of the bovine oocyte.

3.2. On-chip enucleation of the oocyte

Photographs of typical results for the on-chip enucleation are shown in figure 11. Each process was carried out under bright field observation without the use of fluorescent reagents. The target oocyte was transported to the manipulation point in a microchannel. The microgripper then grasped the oocyte. The ZP of the oocyte was slit by the microknife tip and the cytoplasm was pushed out of the ZP. The enucleated oocytes are shown in figure 12(*a*). The enucleated oocytes are spherical, indicating that the cell membrane of the oocytes remained intact. To confirm the success of enucleation using this method, we investigated the viability of oocytes after enucleation. The enucleated oocytes were cultured in 10% FBS with M199 with 6DMAP for 4 h, and then transplanted into a cloned nucleus and cultured for 5 d. Presently, the production rate, i.e. the ratio between the number of oocytes that reach the blastocyst stage and the number of bovine oocytes after nucleus transfer, is 100%.

4. Conclusion

We proposed novel on-chip enucleation of an oocyte with ZP by a combination of untethered microrobots. Enucleation is a cloning technique that can be subdivided into three steps: (a) holding, (b) slitting, and (c) removing the nucleus. To achieve these steps in the closed space of a microfluidic chip, two microrobots, a microknife and a microgripper were integrated into a microfluidic chip by considering the required DOF of motion in each step. These microrobots were actuated by an external magnetic force produced by permanent magnets placed on the robotic stage.

The tip of the microknife was designed by considering the biological geometric feature of an oocyte, i.e., the oocyte has a polar body in maturation stage II. Moreover, the microknife was fabricated using grayscale lithography, which allows the fabrication of 3D microstructures. The microgripper was designed to have a gripping function that is independent of the driving mechanism. The gripping function is performed by the deformation of beams because it is difficult to achieve an ideal microscale hinge-and-link structure. The fabricated microgripper was evaluated and the results show that the measured standard deviation of the positioning accuracy is less than 5 μm, and that there is a relatively linear relationship between the tip displacement and applied voltage when the applied voltage is between –20 V and +20 V.

On-chip enucleation was demonstrated under bright field observation without the use of fluorescent reagents. The enucleated oocytes are spherical, indicating that the cell membrane of the oocytes remained intact. To confirm successful enucleation using this method, we investigated the viability of oocytes after enucleation. Presently, the production rate is 100%.

The proposed untethered microrobots will contribute to complex cell manipulation, such as cell surgery, in the closed space of lab-on-a-chip devices because the microrobots are disposable and permit noncontact actuation. In the future, we will develop an automated enucleation system for high-throughput cloning.

Acknowledgement

This work was supported by JST SENTAN, a Grant-in-Aid for Scientific Research from the Ministry of Education, Culture, Sports, Science and Technology (25630090), and the Japan Society for the Promotion of Science.

References

[1] Vogel A *et al* 2005 Mechanisms of femtosecond laser nanosurgery of cells and tissues *Appl. Phys.* B **81** 1015–47
[2] Hosokawa H *et al* 2003 Fabrication of nanoscale Ti honeycombs by focused ion beam *Mater. Sci. Eng.* **A344** 365–7
[3] Wilmut I *et al* 1997 Viable offspring derived from fetal and adult mammalian cells *Nature* **385** 810–3
[4] Wakayama T *et al* 1998 Full-term development of mice from enucleated oocytes injected with cumulus cell nuclei *Nature* **394** 369–74
[5] Watanabe S (ed) 2011 *Manual for the Enucleation of Bovine Oocyte And Evaluation of Quality of Embryo No.9* (National Institute of Livestock and Grassland Science Technical Report) 5 (ISSN 1347–2712)
[6] Yamanishi Y *et al* 2010 Design and fabrication of all-in-one unified microfluidic chip for automation of embryonic cell manipulation *J. Robot. Mechatron.* **22** 371–9
[7] Ichikawa A *et al* 2011 Automatic cell cutting by high-precision microfluidic control *J. Robot. Mechatron.* **23** 13–8
[8] Feng L, Hagiwara M, Ichikawa A and Arai F 2013 On-chip enucleation of bovine oocytes using microrobot-assisted flow-speed control *Micromachines* **4** 272–85
[9] Wassarman P M 2008 Zona pellucida glycoproteins *J. Biol. Chem.* **283** 24285–9
Feng L, Hagiwara M, Ichikawa A and Arai F 2013 On-chip enucleation of bovine oocytes using microrobot-assisted flow-speed control *Micromachines* **4** 272–85
[10] Wassarman P M 2008 Zona pellucida glycoproteins *J. Biol. Chem.* **283** 24285–9
[11] Hu W *et al* 2011 Micro-assembly using optically controlled bubble microrobots *Appl. Phys. Lett.* **99** 094103
[12] Arai F *et al* 1999 Selective manipulation of a microbe in a microchannel using a teleoperated laser scanning manipulator and dielectrophoresis *Adv. Robot.* **13** 343–5
[13] Hagiwara M *et al* 2011 Precise control of magnetically driven microtools for enucleation of oocytes in a microfluidic chip *Adv. Robot.* **25** 991–1005

[14] Barbic M, Mock J J, Gray A P and Schultz S 2001 Electromagnetic micromotor for microfluidics applications *Appl. Phys. Lett*. **79** 1399–401
[15] Mensing G A, Pearce TM, Graham M D and Beebe D J 2004 An externally driven magnetic microstirrer *Phil. Trans. R. Soc. Lond. A Math. Phys. Eng. Sci*. **362** 1059–68
[16] Yamanishi Y, Sakuma S, Onda K and Arai F 2008 Powerful actuation of magnetized microtools by focused magnetic field for particle sorting in a chip *Biomed. Microdevices* **10** 411–9
[17] Hagiwara M, Kawahara T, Iijima T and Arai F 2013 High-speed magnetic microrobot actuation in a microfluidic chip by a fine v-groove surface *IEEE Trans. Robot.* **29** 363–72
[18] Sakuma S *et al* 2013 Cellular force measurement using a nanometric-probe-integrated microfluidic chip with a displacement reduction mechanism *J. Robot. Mechatron.* **25** 277–84
[19] Waits CM *et al* 2008 Microfabrication of 3D silicon MEMS structures using gray-scale lithography and deep reactive ion etching *Sensors and Actuators* A **119** 245–53